Stanford Exploration Project, Report 113, July 8, 2003, pages 221–231

Angle decompositions of images migrated by wavefield extrapolation

Paul Sava[1]

ABSTRACT

I present an extension to the angle-domain decomposition of images migrated using wavefield extrapolation. Traditionally, reflectivity is described by a 1-D function of scattering angle. I show that we can further decompose the image function of other angles related to the structure and acquisition. In the 2-D case, the reflectivity is described function of two angles, while in the 3-D case the reflectivity is described function of four angles. Applications for such a multi-angle decomposition include amplitude and illumination compensation due to limited acquisition.

INTRODUCTION

Angle-domain common image gathers (ADCIGs) are decompositions of seismic images in components proportional to the reflection magnitude at various incidence angles at the reflector. ADCIGs can be constructed for many types of methods, including Kirchhoff, one-way wavefield extrapolation or two-way reverse time migration. The main applications of ADCIGs are in migration velocity analysis (MVA) and amplitude versus angle analysis (AVA).

Generally speaking, there are two classes of ADCIGs: those computed in the data space, which produce images with reflectivity described as a function of offset ray parameter p_h (de Bruin et al., 1990; Prucha et al., 1999) and those computed in the image space, which produce images with reflectivity function of scattering angle γ (Weglein and Stolt, 1999; Sava and Fomel, 2003).

The mechanics of computing angle-gathers with either of these two methods are similar, since both involve slant-stacks or radial-trace transforms at various stages of the wavefield extrapolation migration, before or after imaging.

The main advantages and disadvantages of the two methods are discussed by Sava and Fomel (2003). The most important advantage of the image space method over the data space method is its versatility: the same transformation can be used for images produced by shot-geophone (S-G) migration (Sava and Fomel, 2003), shot-profile migration (Rickett and Sava, 2001), reverse-time migration (Biondi and Shan, 2002), and even for migrated images of converted waves (Rosales and Rickett, 2001). In all cases, we obtain at every point in the image

[1]**email:** paul@sep.stanford.edu

a 1-D description of the reflection magnitude function of the scattering angle (γ), measured with respect to the normal to the reflector.

However useful, this ADCIG transformation is incomplete. There are situations when by observing how reflectivity changes with the scattering angle, we cannot distinguish among totally different geologic scenarios. A striking comparison is that between a reflector and a diffractor which are both kinematically represented by flat gathers.

This paper presents a simple extension to the angle-gather transformation. By employing similar techniques as the ones used for the more traditional approach, we can create ADCIGs where reflectivity is described by two parameters in 2-D, or by four parameters in 3-D. These angles represent the structural dip, acquisition azimuth and scattering angles. Using simple examples, I show that this more complex decomposition is capable of highlighting new and useful information. Possible applications of this decomposition include illumination compensation due to limited acquisition, or dip-dependent migration amplitude corrections (Sava et al., 2001).

2-D THEORY

The derivation in this section follows the one of Fomel (1996). Assuming that a reflection event in the extrapolated wavefield is described by the function $t(z,s,r)$, we find from the Snell's law the following derivatives:

$$\frac{\partial t}{\partial s} = \frac{\sin(\alpha-\gamma)}{v}\,, \tag{1}$$

$$\frac{\partial t}{\partial r} = \frac{\sin(\alpha+\gamma)}{v}\,, \tag{2}$$

where s,r stand for the source and receiver spatial coordinates, v is the wave velocity, α is the dip angle, and γ is the reflection angle (Figure 1). The traveltime derivative with respect to

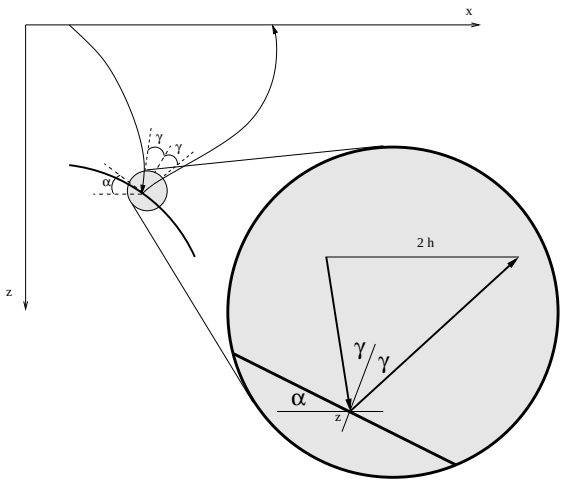

Figure 1: A sketch of reflection rays in an arbitrary-velocity medium. paul3-local [NR]

the depth of the observation surface z has contributions from the two branches of the reflected

ray, as follows:

$$\frac{\partial t}{\partial z} = \frac{\cos(\alpha-\gamma)}{v} + \frac{\cos(\alpha+\gamma)}{v}\,. \tag{3}$$

Equation 3 corresponds to the well-known double-square-root equation (Claerbout, 1985). This equation simply reflects the fact that the traveltime increases with increasing depth of the reflector.

Transforming Equations (1-3) to the midpoint and half-offset coordinates, we obtain

$$\frac{\partial t}{\partial x} = \frac{\partial t}{\partial s} + \frac{\partial t}{\partial r} = \frac{2\sin\alpha\,\cos\gamma}{v}\,, \tag{4}$$

$$\frac{\partial t}{\partial h} = \frac{\partial t}{\partial r} - \frac{\partial t}{\partial s} = \frac{2\cos\alpha\,\sin\gamma}{v}\,, \tag{5}$$

$$\frac{\partial t}{\partial z} = -\frac{2\cos\alpha\,\cos\gamma}{v}\,. \tag{6}$$

At a fixed image location x, we can transform the derivatives of $t(z,x,h)$ to the derivatives of $z(t,x,h)$ by applying the implicit function theorem. Using Equations (5-6), we obtain

$$\frac{\partial z}{\partial h} = -\frac{\partial t}{\partial h}\Big/\frac{\partial t}{\partial z} = -\tan\gamma, \tag{7}$$

and using Equations (4-6), we obtain

$$\frac{\partial z}{\partial x} = -\frac{\partial t}{\partial x}\Big/\frac{\partial t}{\partial z} = -\tan\alpha. \tag{8}$$

Sava and Fomel (2003) use Equation (7) to compute angle-domain common image gathers for images obtained by wavefield extrapolation. This formula can be implemented either as a slant-stack in the space domain, or as a radial-trace transform in the Fourier domain. In both cases, we obtain at every point in the image the reflection strength as a function of scattering angle, independent of the reflector dip.

Similarly, we could employ formula (8) for another decomposition of the migrated image function of the structural dip α. As for equation (7) which represents a slant-stack in the $x-h$ plane, equation (8) represents a slant-stack in the $x-z$ plane (Figure 2).

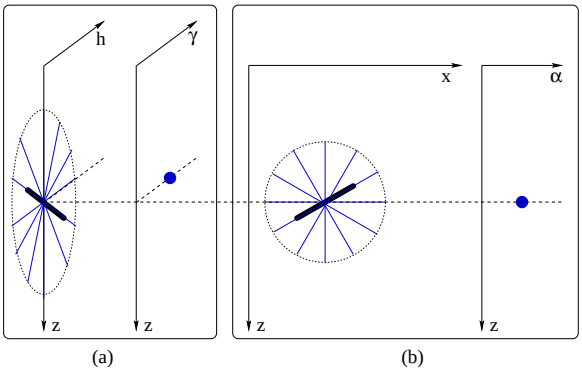

Figure 2: Angle decompositions. Panel (a) corresponds to slant-stack angle-decomposition in the $z-h$ plane. Panel (b) corresponds to slant-stack angle-decomposition in the $z-x$ plane. In both cases, a dipping segment maps at a particular angle. paul3-sls [NR]

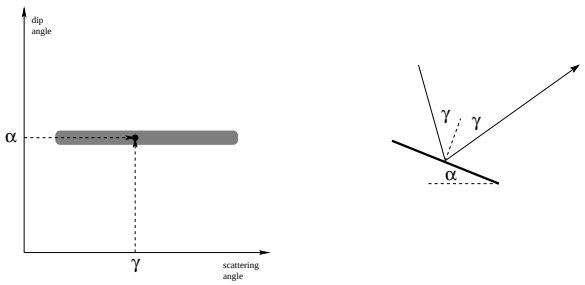

Figure 3: A sketch of a generic reflection experiment and its associated angle decomposition. The left panel corresponds to the $x-z$ location of the reflection point in the image. In the 2-D case, at every point in image, the reflectivity is described by two angles, α and γ. paul3-mag [NR]

3-D THEORY

Equations (7) and (8) are derived with the assumption of a 2-D earth. As pointed out by Tisserant and Biondi (2003), the Fourier-domain angle-gather transformation

$$\tan\gamma = -\frac{k_h}{k_z} \tag{9}$$

is not valid in general in 3-D and needs to be corrected for the crossline dip component of the structure.

Tisserant and Biondi (2003) show that we can make this 3-D correction by re-writing the angle-gather transformation as

$$\tan\gamma = -\frac{|\mathbf{k}_h|}{k_z}\frac{1}{\sqrt{1+\left(\frac{k_{mx}}{k_z}\sin\beta+\frac{k_{my}}{k_z}\cos\beta\right)^2}}, \tag{10}$$

where β is the acquisition azimuth, $|\mathbf{k}_h|$ is the absolute value of the offset wavenumber, and k_{mx}, k_{my} are the components of the midpoint wavenumber. If we introduce the notation $\tan\delta_x = -\frac{k_{mx}}{k_z}$ and $\tan\delta_y = -\frac{k_{my}}{k_z}$, we can write

$$\tan\gamma = -\left[\frac{1}{\sqrt{1+\left(\tan\delta_x\sin\beta+\tan\delta_y\cos\beta\right)^2}}\right]\frac{|\mathbf{k}_h|}{k_z}. \tag{11}$$

δ_x and δ_y represent the projection angles of the normal to the reflection plane onto the Cartesian coordinate system. Equation (11) gives the relation between the four angles describing the reflectivity decomposition in 3-D, namely the structural dip angles (δ_x, δ_y), the recording azimuth (β), and the scattering angle (γ).

The 3-D decomposition algorithm is based on the following scheme:

- Begin from a 3-D migrated image

$$R(z, h_x, h_y, m_x, m_y). \tag{12}$$

Transform it to polar coordinates in the $h_x - h_y$ plane

$$R(z, h, \beta, m_x, m_y), \tag{13}$$

where, by definition, $\tan\beta = -\frac{k_{hy}}{k_{hx}}$ and $h = \sqrt{h_x^2 + h_y^2}$.

- Decompose the image by dip and dip azimuth, or equivalently by the projections of the normal to the reflection plane on the Cartesian axes (δ_x, δ_y):

$$R(z, h, \beta, \delta_x, \delta_y), \tag{14}$$

where $\tan\delta_x = -\frac{k_{mx}}{k_z}$ and $\tan\delta_y = -\frac{k_{my}}{k_z}$.

- At every $\beta, \delta_x, \delta_y$, decompose the image function of scattering angle γ

$$R(z, \gamma, \beta, \delta_x, \delta_y) \tag{15}$$

using Equation (11).

The four angles describing reflectivity are just one particular and convenient choice. Any other convenient quartet of angles can be used, although such alternatives yield no new information.

EXAMPLES

The first example, Figures 4 and 5, is a fairly simple synthetic model populated with reflectors at various dips and a few diffractors. One goal of this model is to demonstrate the ability of the transformation described in this paper to distinguish reflections from diffractions.

Figure 5 shows on the left a typical ADCIG. Clearly, this panel does not allow us to distinguish reflectors from diffractors. However, the dual angle decomposition presented in the right panels for two particular depths at the same location show a clear distinction between reflectors and diffractors: either the event concentrates around the dip direction (reflections), or it maps uniformly to all dips (diffractions).

Figure 6 is a summary of the multi-angle decomposition for the entire synthetic model. Each rectangle represents an image point located roughly at the same location of the rectangle. In each box, the horizontal axis corresponds to the dip angle α, and the vertical axis corresponds to the scattering angle γ.

The second example concerns the well known Marmousi model. Figures 7 depicts the migrated image, and the vertical line indicates the location of the ADCIG under analysis. Figure 8 shows on the left a standard 1-D ADCIG, and on the right the multi-angle decomposition for two particular depths at the same location. Each one of the right panels shows events dipping in opposite directions at different angles. In this example, the dip angle decomposition is not as sharp as in the preceding model due to the limited resolution of the space-domain slant-stacks. Nevertheless, the selected events are clearly located at different structural dip angles.

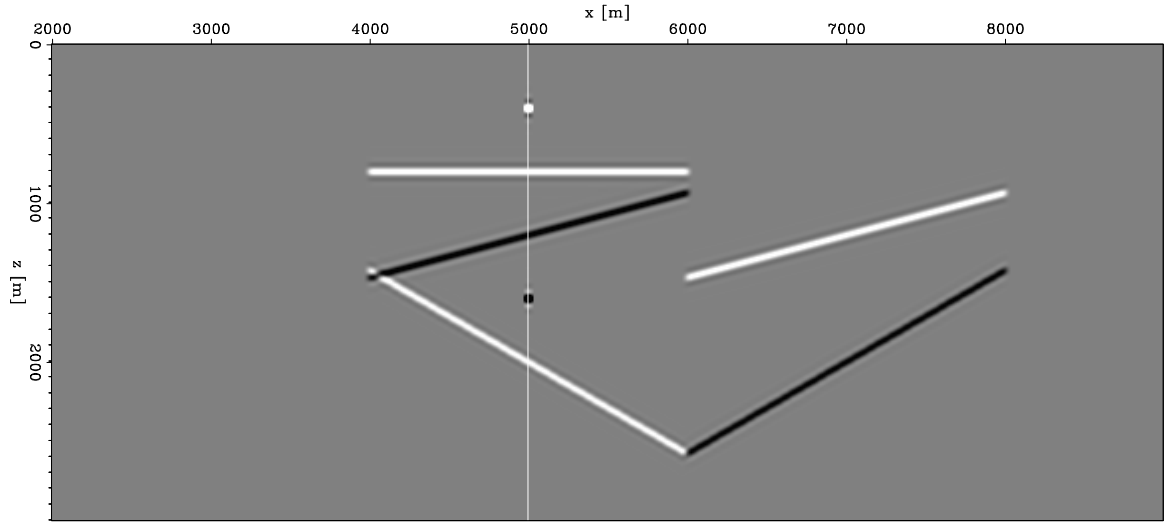

Figure 4: Model image with perfectly imaged reflectors and diffractors. paul3-imag1 [CR]

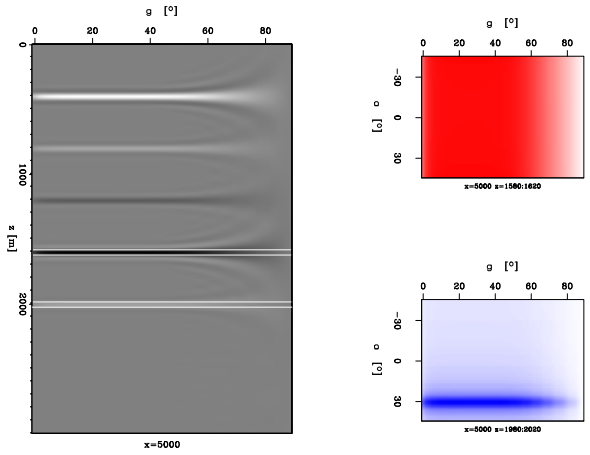

Figure 5: Image decomposition by scattering angle γ (left). Image decomposition by scattering angle γ and dip α angle (right) at the depth levels marked on the left panel. The top-right panel corresponds to a diffractor, and the bottom-right panel corresponds to a reflector dipping at 30 degrees. paul3-comb1 [CR]

The next example corresponds to a 3-D seismic image (Figure 9) obtained by narrow-azimuth migration (Biondi, 2003). The figure depicts the zero offset $h_x = 0, h_y = 0$ image, although in reality the cube has the full 5 dimensions of 3-D prestack data.

I decompose the reflectivity at $m_x = 1000, m_y = 800$ function of the four angles introduced in the preceding section. This 4-D image decomposition is practically impossible to fully illustrate on paper. A reasonable alternative is to display subsets of the decomposition, by appropriate summation over some of the angles. For example, Figure 10 shows an usual angle gather, obtained by summation over the reflector dip angles δ_x, δ_y and acquisition azimuth β. The left panel depicts an angle gather computed using the 2-D formula, and the right panel shows an angle gather at the same location obtained by summation of the three angles after the 3-D image decomposition. As also seen by Tisserant and Biondi (2003), not much changes for the upper flat reflector, but the event for the bottom reflector shrinks according to the crossline structural dip.

The more interesting plots, however, concern other partial summations over the four an-

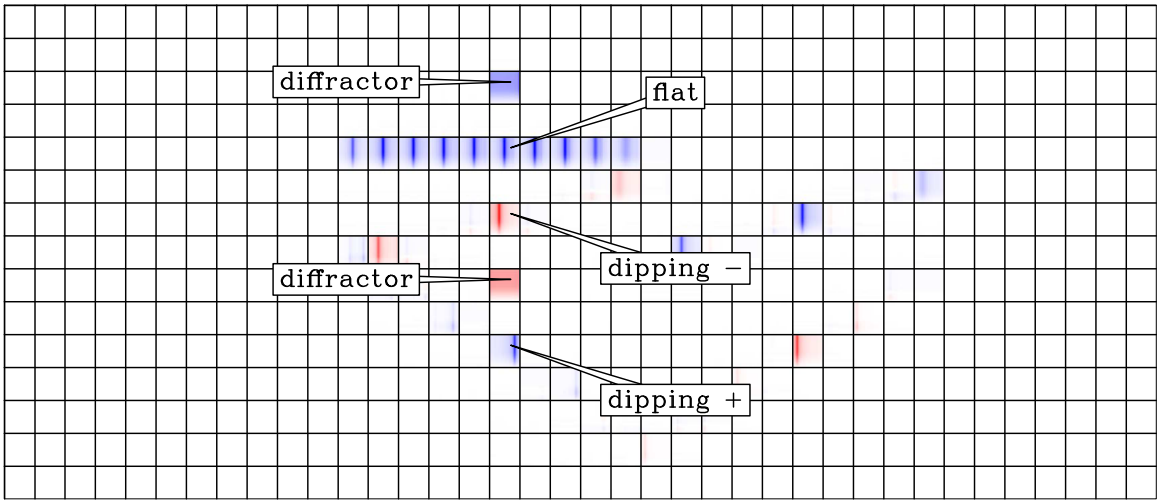

Figure 6: Multi-angle decomposition for the image in Figure 5. In each box, the horizontal axis corresponds to the dip angle α, and the vertical axis corresponds to the scattering angle γ. paul3-chck1 [CR]

gles. Figure 11 shows two such partial summations: on the left, the panels correspond to summation over the scattering and azimuth angles (γ and β); on the right, the panels correspond to summation over the projections of the normal to the reflector (δ_x and δ_y). From top to bottom, each pair of panels corresponds to different depths $z = 1000, 1150, 1380$ at the same location in the image $m_x = 1000, m_y = 800$.

The panels on the left simply indicate the dip and azimuth direction of the normal to the reflection plane, measured by its projections on the Cartesian coordinate system. The right panels, however, show the reflectivity variation with scattering angle and acquisition azimuth. The energy is unevenly distributed function of scattering angle and azimuth. Furthermore, the energy decays at higher scattering angles. The effect is similar to that observed by Sava et al. (2001) for traditional 2-D angle-gathers. We can also observe amplitudes decaying with depth, which is consistent with smaller angular coverage for a fixed acquisition geometry.

CONCLUSIONS

An extension to a widely used transformation allows descriptions of migrated images in components corresponding to various dip, scattering and azimuth angles. Two angles are enough to fully describe the imaged reflectivity in the case of a 2-D experiment. In the more general 3-D case, images are described by four angles.

This image transformation has many applications, among which amplitude compensation (Sava et al., 2001) for AVA analysis, and illumination normalization for limited and irregular data acquisition. We could also imagine many other ways of filtering our migrated images in various sub-panels of the 3-D decomposition, to correct or eliminate specific events.

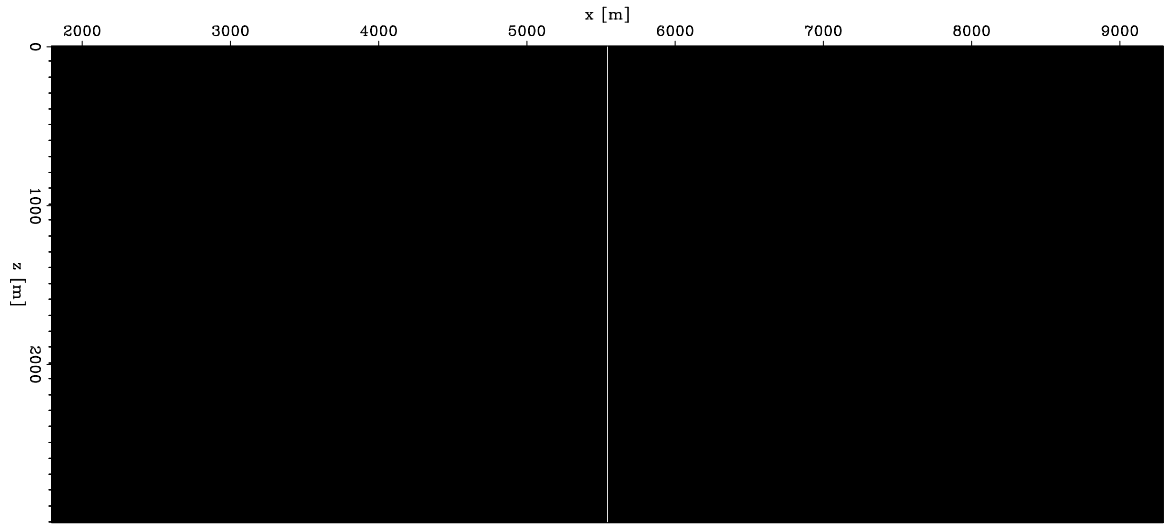

Figure 7: Marmousi model: migrated image. paul3-imagC [CR]

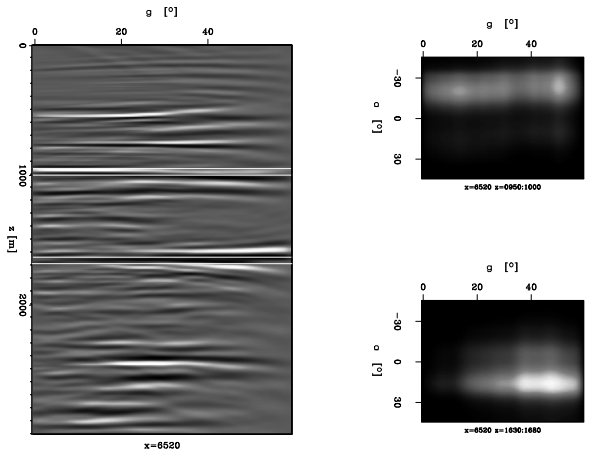

Figure 8: Image decomposition by scattering angle γ (left). Image decomposition by scattering angle γ and dip α angle (right) at the depth levels marked on the left panel. paul3-combC [CR]

Finally, I emphasize that neither the standard nor this extended multi-angle ADCIG transformation add any new information that does not already exist in the migrated image. Both represent decompositions of the image in subsets that are useful and simply more convenient for different applications.

REFERENCES

Biondi, B., and Shan, G., 2002, Prestack imaging of overturned reflections by reverse time migration: 72nd Ann. Internat. Mtg., Soc. of Expl. Geophys., Expanded Abstracts, 1284–1287.

Biondi, B., 2003, Narrow-azimuth migration of marine streamer data: SEP–**113**, 107–120.

Claerbout, J. F., 1985, Imaging the Earth's Interior: Blackwell Scientific Publications.

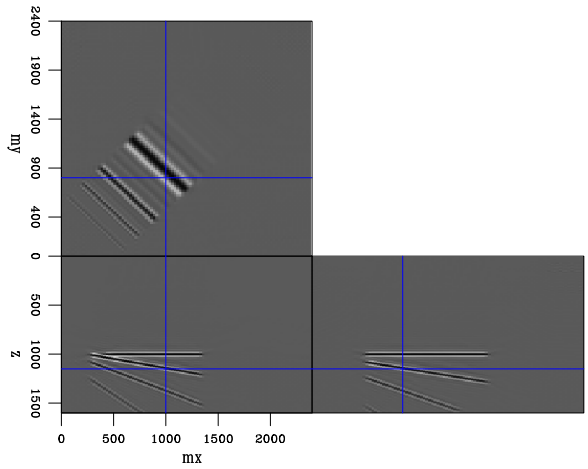

Figure 9: 3-D narrow-azimuth migrated image. The figure depicts the zero offset ($h_x = 0, h_y = 0$) image out of a cube with 5 dimensions. paul3-imag3d [CR]

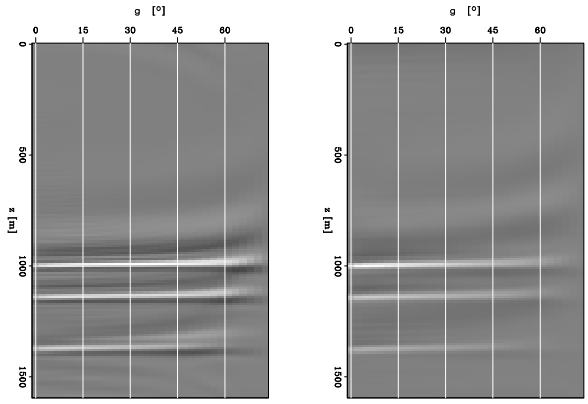

Figure 10: Angle gather obtained by the traditional ADCIG equation (left). 3-D angle gather obtained by summation over the reflector dip angles δ_x, δ_y and acquisition azimuth β (right). paul3-acig3d [CR]

de Bruin, C., Wapenaar, C., and Berkhout, A., 1990, Angle-dependent reflectivity by means of prestack migration: Geophysics, **55**, no. 9, 1223–1234.

Fomel, S., 1996, Migration and velocity analysis by velocity continuation: SEP–**92**, 159–188.

Prucha, M., Biondi, B., and Symes, W., 1999, Angle-domain common-image gathers by wave-equation migration: 69th Ann. Internat. Meeting, Soc. of Expl. Geophys., Expanded Abstracts, 824–827.

Rickett, J., and Sava, P., 2001, Offset and angle domain common-image gathers for shot-profile migration: 71st Ann. Internat. Meeting, Soc. of Expl. Geophys., Expanded Abstracts, 1115–1118.

Rosales, D., and Rickett, J., 2001, PS-wave polarity reversal in angle domain common-image gathers: 71st Ann. Internat. Meeting, Soc. of Expl. Geophys., Expanded Abstracts, 1843–1846.

Sava, P., and Fomel, S., 2003, Angle-domain common-image gathers by wavefield continuation methods: Geophysics, **68**, in press.

Sava, P., Biondi, B., and Fomel, S., 2001, Amplitude-preserved common image gathers by

wave-equation migration: 71st Ann. Internat. Mtg., Soc. of Expl. Geophys., Expanded Abstracts, 296–299.

Tisserant, T., and Biondi, B., 2003, Wavefield-continuation angle-domain common-image gathers in 3-D: SEP–**113**, 211–220.

Weglein, A., and Stolt, R., 1999, Migration-inversion revisited: The Leading Edge, **18**, 950–952.

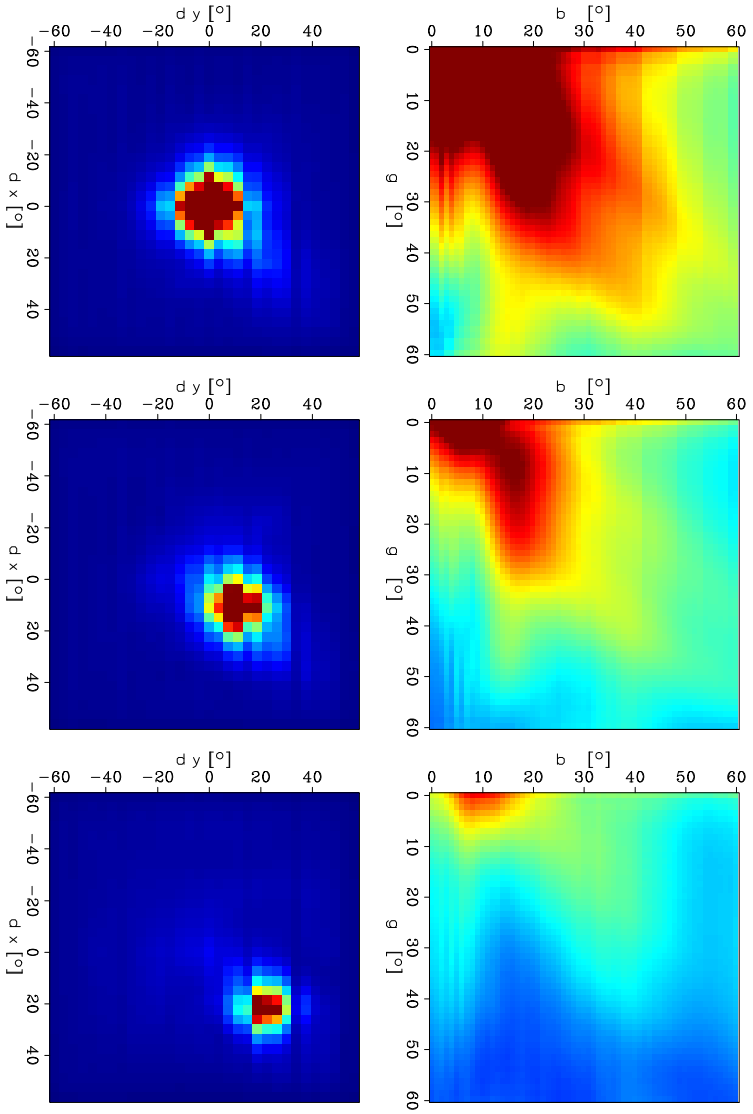

Figure 11: 3-D multi-angle decomposition of migrated images. On the left, the panels correspond to summation over the scattering γ and azimuth β angles. On the right, the panels correspond to summation over the projections of the normal to the reflector, δ_x and δ_y. From top to bottom, each pair of panels corresponds to different depths $z = 1000, 1150, 1380$ at the same location in the image $m_x = 1000, m_y = 800$. paul3-slic3d [CR]